Engineering Structures 253 (2022) 113740

Contents lists available at ScienceDirect

Engineering Structures

journal homepage: www.elsevier.com/locate/engstruct

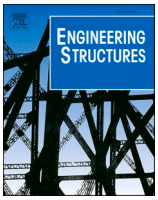

A stiffness reduction method for the in-plane design of stainless steel members and frames according with EN 1993-1-4

Isabel González-de-León *, Itsaso Arrayago, Esther Real, Enrique Mirambell

Universitat Politècnica de Catalunya, Dept. of Civil and Environmental Engineering, Spain

ARTICLE INFO

Keywords:
Global design
Stiffness Reduction Method
Material nonlinearities
Structural members
Frames
Stainless steel

ABSTRACT

Current design standards for stainless steel such as ASCE 8-02 and EN 1993-1-4 prescribe provisions for the design of cross-sections and members that account for material nonlinearities and strain hardening, although these features are not considered in the global design of structures. Recent studies have highlighted the need of accounting for material nonlinearities in order to design efficient and safe stainless steel structures, and it is expected that the forthcoming versions of the standards will incorporate updated rules for the global design of these structures. To contribute to this field, this paper presents a Stiffness Reduction Method (SRM) for the in-plane design of stainless steel members and frames with stocky sections based on the prescriptions given in the next version of EN 1993-1-4. The proposed approach predicts the ultimate capacity and internal forces in stainless steel structures by performing a second-order elastic analysis in which the stiffnesses of the members are reduced by a set of factors defined in this paper to account for the effect of the spread of plasticity, residual stresses and member imperfections. The accuracy of the presented method is assessed for individual stainless steel structural members (columns, beams, and beam-columns) with different cross-sections and material properties, and for austenitic stainless steel portal frames, against numerical results obtained from nonlinear analyses conducted on finite element models. A comparison between the proposed approach and the Direct Analysis Method prescribed in the upcoming AISC 370 Specification is also provided, showing that the results are comparable in the two approaches.

1. Introduction

Stainless steel is increasingly used in structural engineering due to its mechanical properties and excellent corrosion resistance. Design standards for structural stainless steel, based on those prescribed for carbon steel, are progressively more specific and comprehensive, and are aimed at designing more efficient structures. In the recent decades, research efforts have focused on the characterization of the nonlinear stress–-strain response of stainless steel alloys, which differs from the bilinear behaviour exhibited by carbon steel, and on the development of design expressions for stainless steel structural members. In addition, more accurate deformation-based design approaches for stainless steel elements including strain hardening material effects to fully exploit the cross-sectional capacity have been developed, such as the Continuous Strength Method (CSM) [1–3] and the Direct Strength Method (DSM) [4]. Nevertheless, current stainless steel standards, such as the ASCE 8-02 [5] and the European EN 1993-1-4 [6], do not provide specific provisions for the global analysis or design of stainless steel structures, although recent studies have highlighted the need of accounting for material nonlinearities in order to design safer structures [7]. Therefore, research is now being focused on understanding the global behaviour of stainless steel structures [8] and on proposing global design expressions that consider the effects of material nonlinearity [9] or geometric nonlinearity [7,10]. In addition, the forthcoming publication of the European standard prEN 1993-1-14 [11], which regulates the design of steel structures through numerical methods, will allow all types of stainless steel structures to be designed by directly considering geometrical and material nonlinearities and initial imperfections in the analysis (i.e., through GMNIA analysis). Nevertheless, GMNIA analyses require advanced software that is not always available to designers so European researchers have tended to prescribe global design expression alternatives to account for geometric nonlinearities, such as the amplification of horizontal forces in single storey carbon steel [12] and stainless steel [7,13] frames, while research in the US has focused on providing alternative design approaches known as Stiffness Reduction Methods (SRM), which account indirectly for material nonlinearities

* Corresponding author at: Isabel González-de-León, Jordi Girona 1-3, Building C1, 08034 Barcelona, Spain.
E-mail address: isabel.gonzalez.de.leon@upc.edu (I. González-de-León).

https://doi.org/10.1016/j.engstruct.2021.113740
Received 2 June 2021; Received in revised form 21 November 2021; Accepted 5 December 2021
Available online 4 January 2022

through the concept of reduced stiffness but require second-order analyses to be carried out.

The strategy of reducing the stiffness of the members to account for material nonlinearities in the design of structures is widely accepted due to its simplicity and accuracy. Traditionally, the SRM has been developed to be used in conjunction with plastic hinge-based analysis [14–20], and generally involves the modelling of geometric imperfections [14–18]. Suroveck-Maleck and White [21,22] proposed a SRM in which the prediction of the capacity for steel structures was achieved through a second-order elastic analysis where only global imperfections were introduced. To account for the spread of plasticity, including the effect of residual stresses, the stiffnesses of the members were reduced by analytical stiffness reduction factors. With slight modifications, this approach was first adopted in 2005 as an annex of the AISC 360 Specification for Structural Steel Buildings [23] as the Direct Analysis Method (DM). In the following editions of this Standard, the DM has become the preferred design method and has been incorporated in the main body of the Specification because it provides accurate estimates of the load effects in all types of steel structural systems and eliminates the need of calculating effective buckling lengths [24]. In the DM, the estimations of strengths are obtained from a second-order elastic analysis where the spread of plasticity is taken into account by reducing the stiffness of the members by two reduction factors: a general stiffness factor applied to the whole structure, and an additional factor only affecting the flexural stiffness of the members contributing to the stability of the structure. Initial global imperfections (out-of-plumbness of columns) should always be included in the analysis by means of notional loads or by modelling them directly, while different alternatives exist regarding initial member (out-of-straightness) imperfections: (1) they do not need to be explicitly included in the structural analysis, but they are accounted for by carrying out member checks, or (2) they can be explicitly included in the structural analysis, and therefore only cross-section checks are necessary. The first edition of the American Specification for Structural Stainless Steel Buildings AISC 370 [25] has adapted the DM approach previously developed for carbon steel to stainless steel structures by calibrating new values of the two reduction factors [26]. The other requirements of the DM remain unchanged, i.e., the consideration of initial global imperfections and the verification of member or cross-section strength depending on the approach adopted for the inclusion of member imperfections in the structural analysis. The simplicity and accuracy of Stiffness Reduction Methods (SRM) have driven their adaptation into the European framework [27,28], including the proposal by Kucukler et al. [29,30] for the in-plane design of carbon steel structures and members. As in the DM, global imperfections must be included and cross-section capacities must be checked in the SRM approach proposed in [29,30], but no member checks are required since the proposed stiffness reduction factors are derived from the European buckling curves given in EN 1993-1-1 [12] and are thus implicitly present in the calibrated reduction factors. In this context, the present paper adapts the SRM proposed in [29,30] to stainless steel members and planar structures considering the provisions given in the upcoming version of European standard prEN 1993-1-4 [13]. Therefore, the SRM developed herein estimates second-order plastic forces in stainless steel structures through elastic geometrically nonlinear analyses considering global imperfections with reduced member stiffness to account for material nonlinearities, member imperfections and residual stresses, without requiring running a full GMNIA analysis. The study includes stocky Rectangular Hollow Section (RHS) members made of austenitic, ferritic and duplex stainless steel alloys. The development and assessment of the reduction factors proposed are based on the numerical models detailed in Section 2. In Sections 3 and 4, the development of the expressions to determine the stiffness reduction factors for columns subjected to pure compression and for beams under uniaxial bending, respectively, are presented. In Section 5, the stiffness reduction factor for members subjected to axial load plus bending moment is derived and assessed, and in Section 6 the proposed SRM is applied to different stainless steel planar portal frames subjected to vertical and horizontal loads to evaluate the accuracy of the proposed reduction factors. Finally, the validation of the method is assessed and discussed by comparing the results with those predicted by other design methodologies.

2. Finite element modelling

2.1. General

In this Section, the Finite Element (FE) models used for the assessment and validation of the proposed Stiffness Reduction Method (SRM) are described. The assessment and validation required different types of analysis:

- second-order plastic analysis with imperfections (GMNIA) to recreate the actual behaviour of the structural members and to obtain the target strength values (to be compared with the SRM),
- first-order elastic analysis (LA) and second-order elastic analysis with stiffness reduction (GNA-SR) (to implement the SRM).

The assessment was made on stainless steel columns, beams, beam-columns, and frames, and two types of numerical models were developed with the general-purpose software ABAQUS [31]. GMNIA analyses of structural members were performed on shell-type FE models capable of realistically reproducing local buckling effects, while GNA-SR and LA analyses were conducted on beam-type FE models. For computational efficiency reasons, beam-type FE models were chosen for GMNIA, LA and GNA-SR analyses of portal frames. The modified Riks method available in ABAQUS [31] was used to solve all the FE analyses.

2.1.1. Benchmark models for stainless steel members

Shell FE models of stainless steel columns, beams and beam-columns were developed using four-noded shell elements, denoted as S4R [31], and used in conjunction with GMNIA analyses to estimate the actual capacity of the investigated members. The use of S4R elements together with a GMNIA analysis is widely accepted to reproduce accurately the behaviour of cold-formed steel [32] and stainless steel [33,34] members. After a mesh convergence study, flat regions were discretised following a uniform mesh size of 10 mm, while the curved corner regions were divided into a four-element mesh. Local imperfections were included in the form of the local buckling mode obtained from prior linear elastic eigenvalue buckling analyses with the amplitudes proposed by Gardner and Nethercot [35].

In the case of columns and beam-columns, initial member imperfections were also incorporated following a half sinusoidal shape using the corresponding buckling mode with an amplitude equal to $L_c/1000$, where L_c is the length of the member. Pin-ended boundary conditions were defined by means of kinematic coupling constraints between the end sections of the members and reference points contained in the plane of the cross-sections, to which boundary conditions and loading arrangements were assigned. All degrees of freedom, except the rotation around the minor axis, were constrained at the lower reference point. Similar boundary conditions were assigned to the upper reference point, but the longitudinal displacement was also allowed, and the load was applied as an imposed vertical displacement. While the reference points were located at the centroid of the cross-sections in the models for columns, in the beam-column models both reference points were shifted horizontally to simulate eccentric loads.

Beams were modelled following the four-point bending test configuration (4PB). The loading and support sections were defined as regions forced to move as rigid bodies, placed at the bottom flange of the beams and connected to reference points located at the centre of each region. A more detailed description of these regions is provided in [4,36]. The support reference points were placed 1500 mm apart, according to the loading scheme described in [37], while the loading reference points were placed at a distance of 510 mm from the ends of the members. The

loads were applied as imposed vertical displacements at the loading reference points. The longitudinal and out-of-plane displacements were restrained at the midspan cross-sections, while only the vertical displacement was constrained at the support reference points.

2.1.2. Benchmark models for stainless steel frames

Numerical models of the frames used as benchmarks in Section 6 were analysed by performing a GMNIA analysis and were developed by using Timoshenko linear B21 elements [31], since S4R elements are too computationally expensive for a parametric study [7,10,38]. Each member of the frame was divided into 100 finite elements and cross-sections were defined using the default box-section option in ABAQUS [31]. It is worth mentioning that, in practice, a much smaller number of finite elements than the 100 elements adopted in this study can be used to model individual structural elements. As suggested in [30], four elements may be sufficient for sway structures, while sixteen elements may be required for non-sway structures. Initial global imperfections were included through notional horizontal loads assuming an out-of-plumb angle of 1/200 according to EN 1993-1-1 [12], while the member imperfections of the columns were introduced by directly modifying the position of the nodes following a half-sine wave shape with an amplitude of L_c/1000 in the most detrimental direction. Finally, both fixed- and pin-ended boundary conditions were adopted at the supports of the columns, while vertical and horizontal concentrated loads were applied simultaneously at the top of the columns, as per in the numerical portal frames developed in [10], which were in turn based on the tests reported in [8].

2.1.3. Models for stainless steel members and frames using the Stiffness Reduction Method

For all the FE models carried out using the Stiffness Reduction Method (including columns, beams, beam-columns, and frames), LA and GNA-SR analyses were performed on models using Timoshenko linear in-plane beam elements B21 [31]. In the case of GNA-SR analyses, the cross-section geometry was defined using the generalized-section available in ABAQUS [31]. Generalized-sections allow reducing the moment of inertia (I) without modifying the nominal cross-section area (A) and the material properties, i.e., the Young's modulus (E), so that the flexural stiffness (EI) is modified while the axial stiffness of the members (EA) remains constant [30]. Members were divided into 100 elements. Although the proposed stiffness reduction factor for columns already incorporates the effect of member imperfections, to ensure that the geometrical nonlinearities were triggered in the column models, an imperfection amplitude of 0.001% L_c was incorporated following a half sinusoidal shape [9]. In the case of frames, notional horizontal loads were applied assuming a drift angle of 1/200, as recommended in EN 1993-1-1 [12], in both LA and GNA-SR analyses. The loads were applied as imposed displacements and the boundary conditions were defined following the configurations described above.

2.2. Material model

In both shell and beam FE models, nonlinear material properties were defined by assigning user-defined true stress-plastic strain curves according to the two-stage Ramberg-Osgood material model proposed in [40] and shown in Eq. (1) and Eq. (2), where ε is the strain, σ is the stress, E is the Young's modulus, f_y and f_u are the yield stress and ultimate tensile strength, respectively, ε_u is the ultimate strain, n and m are the strain hardening exponents and E_y is the tangent modulus at the yield stress, given in Eq. (3).

$$\varepsilon = \frac{\sigma}{E} + 0.002\left(\frac{\sigma}{E}\right)^n \quad \text{for } \sigma \le f_y \tag{1}$$

$$\varepsilon = 0.002 + \frac{f_y}{E} + \frac{\sigma - f_y}{E_y} + \varepsilon_u\left(\frac{\sigma - f_y}{f_u - f_y}\right)^m \quad \text{for } f_y < \sigma \le f_u \tag{2}$$

$$E_y = \frac{E}{1 + 0.002n\frac{E}{f_y}} \tag{3}$$

The study presented in this paper was based on austenitic, ferritic and duplex stainless steel RHS members. Table 1 summarises the key weighted average material properties considered, which were calculated according to [35] from the material properties reported in [41] for the flat and corner regions of stainless steel RHS sections. Weighted average material properties were assigned to all the FE models to facilitate the comparison between GMNIA and GNA-SR analyses.

2.3. Validation of FE models

Numerical models for structural members (columns, beams and beam-columns) were validated using shell-type FE models, while the numerical models for portal frames were validated using both shell-type and beam-type FE models, as described in this Section.

The FE models of stainless steel members used in the present study were validated against the experimental results on cold-formed EN 1.4301 austenitic columns and beams with RHS cross-sections reported in [37]. The accuracy of the FE model for columns was assessed by comparing the results of the GMNIA analysis with those of columns subjected to pure compression under pin-ended boundary conditions. The cross-sections were modelled using S4R elements and divided into corner regions and flat regions [35]; the measured material properties given in [37], using the model given in Eq. (1) and Eq. (2), were assigned to each region. For this particular validation, the reference points connected to the end cross-sections were placed at a distance of 50 mm, following the experimental setup. Local and global imperfections were included by using the corresponding buckling modes and the measured amplitudes reported in [37]. To validate the numerical models of the beams, experimental results from four-point bending tests, with the stainless steel RHS sections bent around their major axis, were used. The same type of S4R elements and material models used for columns were also employed for beams. The test setup coincided with that described above for the numerical models of beams, whereby the distance between the support reference points was 1500 mm and between the load reference points, 510 mm. Local imperfections were included using the pattern given by the relevant buckling modes and with the amplitudes measured from the test specimens, as given in [37]. Fig. 1 presents the experimental load-lateral deflection curves of columns under pure compression around major (S2) and minor (S3) axis and the experimental load-midspan deflection curves for beams subjected to major axis bending, compared to the corresponding FE curves. The results demonstrate that the numerical analysis approach used in the present study can accurately simulate the actual behaviour of stainless steel members. It was observed that the failure modes also concurred. Therefore, the use of the numerical analysis approach presented herein is appropriate to obtain reference data to be compared with the results predicted from the proposed Stiffness Reduction Method.

The frame FE model used herein was developed for a previous study and its validation, which was also carried out by comparing the loads and displacements predicted numerically with the corresponding experimental results from the frame tests conducted by Arrayago et al. [8], is available in [10]. Note that the setup reported in [8] varies from that adopted in the parametric study mainly in the position of the loads, the application of the vertical and horizontal loads in two separate steps

Table 1
Key material characterization parameters for parametric studies.

Stainless steel type	E [GPa]	f_y [MPa]	f_u [MPa]	ε_u [mm/mm]	n	m
Austenitic	198	428	650	0.39	5.5	3.7
Ferritic	185	498	520	0.06	11.4	3.1
Duplex	201	707	874	0.36	5.6	4.9

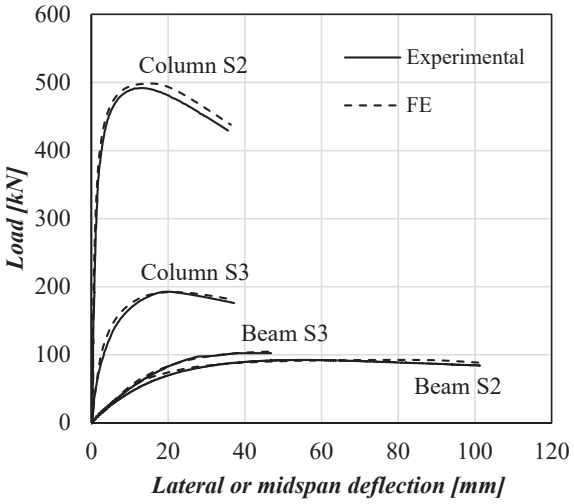

Fig. 1. Comparison of FE load–deflection curves for S2 (RHS 120 × 100 × 4) and S3 (RHS 120 × 40 × 4) austenitic stainless steel columns and four-point bending beams with the experimental results reported in [37].

and the fact that the end support conditions were semi-rigid. Although a detailed model was developed using S4R shell elements, which is described in [8], these experimental and numerical results were used in [10] to validate the computationally more efficient FE models using B21 beam elements. As reported in [10], the experimental and numerical vertical load-midspan deflection curves and the horizontal load–displacement curves showed that the behaviour of stainless steel portal frames with stocky cross-sections could be accurately predicted with a simpler numerical model that used B21 elements.

3. Stiffness reduction under axial loading

In this Section, the development of the stiffness reduction factor τ_N accounting for the loss of stiffness due to geometrical imperfections, residual stresses and the spread of plasticity in stainless steel columns under axial loading is presented, as well as its validation by the comparison of GNA-SR and GMNIA results.

3.1. Derivation of stiffness reduction factor τ_N

The stiffness reduction factor τ_N of a column subjected to axial loading was derived from the European buckling curves specified in the next version of the prEN 1993-1-4 [13] standard and following the methodology proposed by Kucukler et al. [29] for carbon steel columns. The stiffness reduction factor τ_N is the ratio between the inelastic and the elastic critical buckling loads of the member, $N_{cr,i}$ and N_{cr} respectively, and can be expressed in terms of the flexural buckling reduction factor χ and the member slenderness $\bar{\lambda}$, as shown in Eq. (4).

$$\tau_N = \frac{N_{cr,i}}{N_{cr}} = \chi\bar{\lambda}^2 \tag{4}$$

The buckling curves to calculate the flexural buckling reduction factor χ prescribed in the latest edition of the Design Manual for Structural Stainless Steel [42] and in the upcoming version of prEN 1993-1-4 [13] are based on the Ayrton-Perry approach [43]. The buckling reduction factor is given by Eq. (5), where the effects of the residual stresses and member imperfections are included in the auxiliary parameter ϕ defined in Eq. (6). The values of the imperfection factor α and the limiting slenderness $\bar{\lambda}_0$ depend on the type of cross-section, stainless steel family and the buckling axis considered. For the specific case of cold-formed stainless steel RHS columns, the imperfection factor adopts a value of $\alpha = 0.49$ [13,42], while the limiting slenderness is $\bar{\lambda}_0 = 0.3$ for austenitic and duplex stainless steels, and $\bar{\lambda}_0 = 0.2$ for ferritic alloys.

$$\chi = \frac{1}{\phi + \sqrt{\phi^2 - \bar{\lambda}^2}} \quad \text{but } \chi \leq 1.0 \tag{5}$$

where

$$\phi = 0.5\left[1 + \alpha(\bar{\lambda} - \bar{\lambda}_0) + \bar{\lambda}^2\right] \tag{6}$$

The reduction function τ_N proposed herein and given in Eq. (7) and Eq. (8) is adopted from Kucukler et al. [29], which in turn comes from the European buckling curves for carbon steel, but assumes the imperfection factor and limiting slenderness values calibrated for stainless steel alloys [13]. It is noteworthy that the strength prediction resulting from applying the proposed reduction factor τ_N and performing a GNA-SR analysis up to failure is identical to that estimated from the European buckling curve $N_{b,Rk}$. Hence, the maximum column resistance estimated by the proposed SRM is the squash load of the gross cross-section N_{pl}, and the applied axial load N_{Ed} in Eq. (7) and Eq. (8) should not be greater than the characteristic column strength $N_{b,Rk}$.

$$\tau_N = \frac{4\psi^2}{\alpha^{2\frac{N_{Ed}}{N_{pl}}}\left[1 + \sqrt{1 - 4\psi\frac{\left(N_{Ed}/N_{pl} - 1\right)}{\alpha^2 N_{Ed}/N_{pl}}}\right]^2} \quad \text{but} \quad \tau_N \leq 1.0 \tag{7}$$

where

$$\psi = 1 + \bar{\lambda}_0\alpha\frac{N_{Ed}}{N_{pl}} - \frac{N_{Ed}}{N_{pl}} \tag{8}$$

From the relationship presented in Eq. (4), it is possible to derive stiffness reduction functions that consider imperfections and residual stresses based on any buckling curve. For assessment purposes, the stiffness reduction factors derived from the buckling curves proposed in AISC 370 [25] for RHS stainless steel columns were also calculated. Fig. 2 shows the comparison of the stiffness reduction functions specifically obtained herein for austenitic and duplex RHS columns from the buckling curves in prEN 1993-1-4 [13] and AISC 370 [25]. As shown in Fig. 2, both stiffness reduction functions are very similar, as the flexural buckling curves prescribed in AISC 370 [25] have been recently revised to provide strength predictions comparable to those predicted with the European curves [39]. These new buckling curves provide similar or slightly higher strength predictions than the equivalent European curves and show a larger yield plateau due to the less strict reliability requirements stipulated for the AISC 370 Specification. The new expression for the AISC 370 buckling curves is defined in three stages

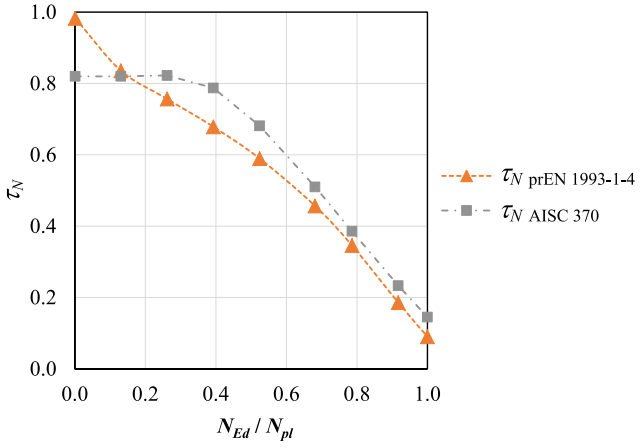

Fig. 2. Comparison between the proposed stiffness reduction factor τ_N and the stiffness reduction factor derived from AISC 370 [25] buckling curves for an austenitic stainless steel column.

depending on the slenderness or stress ratios. For high slenderness ratios, i.e., low N_{Ed}/N_{pl} ratios, the AISC 370 design buckling stress is a constant proportion of the elastic buckling stress, resulting in the plateau shown in Fig. 2 and which adopts a value of 0.82 for austenitic and duplex RHS members.

3.2. Application of the proposed stiffness reduction factor τ_N

The ability of the proposed stiffness reduction factor τ_N based on the European buckling curves for stainless steel RHS columns to consider the effects of material nonlinearities, initial imperfections and residual stresses was evaluated by numerical FE analyses. For this, a range of simply supported columns made of the austenitic, ferritic and duplex materials reported in Table 1 were studied. The geometry of the cross-section considered in the assessment corresponds to the section RHS1 shown in Table 2, where H is the total height of the cross-section, B is the total width, t is the wall thickness and R_{ext} is the external corner radius. Local slenderness values under pure compression $\overline{\lambda}_{p,c}$ are also reported. Table 2 also includes the geometric characteristics of the other cross-sections used in this study (RHS2 and RHS3), and the local slenderness values under major axis bending $\overline{\lambda}_{b,y}$ and minor axis bending $\overline{\lambda}_{b,z}$ for the three cross-sections. All local slenderness $\overline{\lambda}_{p,i}$ values reported in Table 2 were calculated from $\overline{\lambda}_{p,i} = \sqrt{f_y/\sigma_{cr,l}}$, where $\sigma_{cr,l}$ is the elastic local buckling stress of the full cross-section under the appropriate stress distribution, obtained using CUFSM [44]. Finally, the assessment presented in this Section considered different stainless steel columns with varying member lengths, which corresponded to member slenderness values that ranged from 0.25 to 2.00. In total, 8 columns were analysed for each stainless steel family.

The proposed reduction factor τ_N was used to estimate the ultimate strength of the investigated columns by conducting a GNA-SR analysis and its accuracy was assessed by comparing these estimations with the ultimate capacities of the same columns predicted from a GMNIA analysis. The ultimate strength of the columns was estimated as the applied load when the most loaded cross-section reached its cross-section capacity in the GNA-SR analyses proposed in the present study. The ultimate cross-section capacity was determined using the Continuous Strength Method (CSM) interaction equation for RHS cross-sections under combined axial load plus uniaxial bending provided in prEN 1993-1-4 [13], but slightly modified to limit the axial forces up to the squash load of the gross cross-section N_{pl}, since the buckling curves from which the factor τ_N was derived are limited to N_{pl}. The CSM approach is based on the cross-section deformation capacity and provides accurate predictions of the ultimate cross-section resistance because strain hardening effects are taken into account. The CSM formulation relies on a base curve which relates the maximum strain ε_{csm} that a cross-section can experience prior to buckling to its local slenderness $\overline{\lambda}_{p,i}$, normalised by the yield strain ε_y, which is calculated from $\varepsilon_y = f_y/E$. Eq. (9) shows the CSM base curve for fully effective stainless steel cross-sections as given in prEN 1993-1-4 [13], where C_1 is a material coefficient that adopts a value of $C_1 = 0.10$ for austenitic and duplex alloys and $C_1 = 0.40$ for ferritic stainless steel grades, and Ω is a project specific parameter that defines the maximum permissible level of plastic strain in the structure. According to prEN 1993-1-4 [13], the recommended value for Ω is 15.

$$\frac{\varepsilon_{csm}}{\varepsilon_y} = \frac{0.25}{\overline{\lambda}_{p,i}^{3.6}} \leq \min\left(\Omega, \frac{C_1 \varepsilon_u}{\varepsilon_y}\right) \quad \text{for} \quad \overline{\lambda}_{p,i} \leq 0.68 \tag{9}$$

Thus, in the case of stocky cross-sections, the CSM bending moment resistance M_{csm}, whose formulation can be found in the main stainless steel standards and design guides [13,25,42], is greater than M_{pl}. Since RHS1 is a stocky cross-section, the ultimate cross-section resistance of the columns analysed through the GNA-SR proposed herein is that shown in Eq. (10) [13,42]. The parameter a in Eq. (10) depends on the axis of bending and it corresponds to $a = a_w = (A - 2bt)/A$ when calculating the major axis strength and $a = a_f = (A - 2ht)/A$ for minor axis bending, where b and h are the internal width and height of the cross-section, respectively, and A is the cross-sectional area. In the case of RHS sections with local slenderness values $\overline{\lambda}_p > 0.60$, the linear interaction equation given in Eq. (11) might be used. Note that, for comparison purposes, partial safety factors for cross-section γ_{M0} and member γ_{M1} resistances are equal to unity in this paper.

$$M_{Ed} \leq M_N = M_{csm}\frac{1 - \left(N_{Ed}/N_{pl}\right)}{1 - 0.5a} \leq M_{csm} \text{ for } \overline{\lambda}_p \leq 0.60 \tag{10}$$

$$\frac{N_{Ed}}{N_{pl}} + \frac{M_{Ed}}{M_{csm}} \leq 1 \text{ for } \overline{\lambda}_p > 0.60 \tag{11}$$

The results obtained using the proposed stiffness reduction factor τ_N for stainless steel columns are plotted in Fig. 3 along with those corresponding to the stiffness reduction factors derived from the buckling curves proposed in AISC 370 [25], as discussed in Section 3.1. The discrepancies observed between the GNA-SR and GMNIA results are associated with the accuracy or adjustment of the buckling curves considered to the specific stainless steel materials considered in the present study. Both AISC 370 [25] and prEN 1993-1-4 [13] buckling curves were calibrated using a large number of data and provide accurate predictions of the ultimate buckling strengths. Since the proposed τ_N factor was directly obtained from the European buckling curves, the GNA-SR$\tau_{N\ \text{prEN 1993-1-4}}$ curves shown in Fig. 3 overlap the prEN 1993-1-4 [13] buckling curves. Hence, the accuracy of the proposed τ_N factor will depend on the fit of the flexural buckling curves to the ultimate member resistance of stainless steel columns. Based on the results shown in Fig. 3, it can be concluded that the austenitic buckling curve prescribed in prEN 1993-1-4 [13] was in good correlation with the studied austenitic cases, while less accurate fits were found for the ferritic and duplex materials studied.

For the cases considered in this Section, i.e., members under pure compression, it is possible to approximate the inelastic buckling strength of the column by reducing the elastic critical buckling load N_{cr} by τ_N. Furthermore, equivalent results may be obtained when a Linear Buckling Analysis with Reduced Stiffness (LBA-SR) is carried out. The latter

Table 2
Cross-section geometric properties and local slenderness values under different load cases.

Cross-section type	H [mm]	B [mm]	t [mm]	R_{ext} [mm]	Stainless steel type	$\overline{\lambda}_{p,c}$	$\overline{\lambda}_{p,by}$	$\overline{\lambda}_{p,bz}$
RHS1	90.0	76.0	6.0	9.5	Austenitic	0.32	0.25	0.29
					Ferritic	0.36	0.28	0.33
					Duplex	0.41	0.32	0.37
RHS2	125.0	76.0	6.0	9.5	Austenitic	0.43	0.25	0.41
					Ferritic	0.48	0.28	0.46
					Duplex	0.55	0.32	0.52
RHS3	146.0	76.0	6.0	9.5	Austenitic	0.50	0.26	0.48
					Ferritic	0.56	0.29	0.54
					Duplex	0.64	0.33	0.61

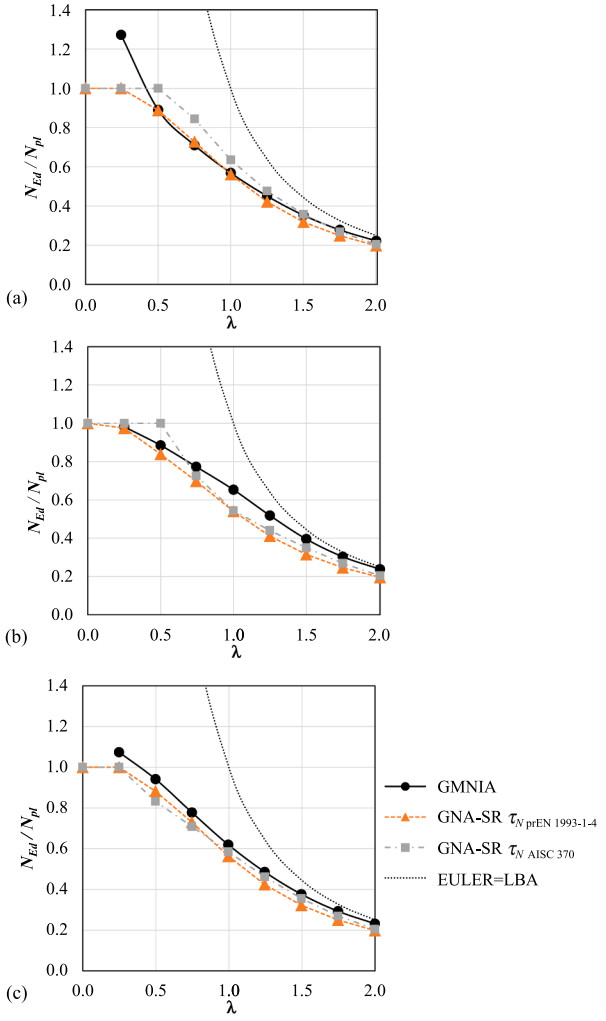

Fig. 3. Comparison of the results obtained from different GNA-SR analyses with GMNIA predictions on (a) austenitic, (b) ferritic and (c) duplex stainless steel simply supported columns.

approach is especially recommended for columns subjected to non-uniform axial forces, with non-uniform cross-section or various boundary conditions [29].

4. Stiffness reduction under bending

In this Section, the derivation of the stiffness reduction function τ_M for estimating the yield distribution effects on the structural behaviour of beams under pure bending through a GNA-SR analysis is presented. Application of the derived τ_M factor and the assessment of the results are also provided.

4.1. Derivation of stiffness reduction factor τ_M

In out-of-plane restrained beams subjected to constant bending moment, the stiffness reduction function τ_M estimates the spread of plasticity in the cross-section and, therefore, it depends on the cross-sectional geometry, material response and residual stresses, but not on the initial geometrical imperfections [29]. The reduction factor τ_M corresponding to a certain bending moment M_{Ed} can be expressed as the ratio between the tangent flexural stiffness at a particular bending moment value EI_t, and the initial flexural stiffness EI. As shown in Eq. (12), the tangent flexural stiffness of a member at any given bending moment value EI_t corresponds to the derivation of $dM_{Ed}/d\kappa$, where κ is the curvature; in other words, to the slope of the moment–curvature curve at M_{Ed}.

$$\tau_M = \frac{EI_t}{EI} = \frac{\frac{dM_{Ed}}{d\kappa}}{EI} \tag{12}$$

Real and Mirambell [45] proposed an analytical expression to describe the bending moment–curvature relationship of stainless steel beams subjected to bending moment up to a moment M_{02}, which corresponds to the moment at which the maximum normal tensile stress is equal to the yield stress f_y. Note that for materials showing nonlinear stress–strain responses such as stainless steels, M_{02} is different from the elastic bending moment of the section and can be estimated by integrating the nonlinear stress distribution of the cross-section [45]. The expression approximates the cross-sectional curvature as a combination of elastic and plastic components. While the elastic component corresponds to the ratio of the applied moment M_{Ed} and the initial flexural stiffness EI, the plastic component is governed by the definition of the plastic curvature $\kappa_{p,02}$ for M_{02}. Recently, Shen and Chacón [9] proposed a stiffness reduction function for stainless steel RHS beams based on Real and Mirambell's approximation. However, the proposed function was only valid up to a moment equal to the elastic moment M_{el}, so a second stage was added to the τ_M formula to consider nonlinear stress distributions up to the plastic moment M_{pl} [9].

In an effort to simplify this approach, the alternative expression for the calculation of the curvature up to M_{pl} given in Eq. (13) is proposed in this paper. Eq. (13) is based on Real and Mirambell's expression but, while the elastic component is the same, the plastic component uses the plastic moment M_{pl} instead of M_{02}, and the plastic curvature κ_p corresponding to M_{pl} is adopted (instead of the $\kappa_{p,02}$ curvature). The plastic curvature κ_p, defined in Eq. (14), can be determined as the difference between the curvatures corresponding to the plastic M_{pl} and elastic M_{el} bending moments. These curvatures are calculated based on the strains and the cross-section half-heights, i.e., $\kappa = \varepsilon/(H/2)$. While the strain for M_{el} is straightforward, that for M_{pl} can be accurately estimated as $3\varepsilon_y$ for RHS, following the recommendations in [4,46].

$$\kappa = \frac{M_{Ed}}{EI} + \kappa_p \left(\frac{M_{Ed}}{M_{pl}}\right)^{n-1} \tag{13}$$

$$\kappa_p = \frac{2}{H}\left(3\varepsilon_y - \varepsilon_y\right) \tag{14}$$

By deriving Eq. (13) with respect to κ, substituting the resulting expression into Eq. (12) and assuming $2\varepsilon_y EI/H = M_{el}$, the stiffness reduction factor τ_M shown in Eq. (15) is obtained.

$$\tau_M = \left[1 + (n-1)\frac{2M_{el}}{M_{pl}}\left(\frac{M_{Ed}}{M_{pl}}\right)^{n-2}\right]^{-1} \tag{15}$$

The τ_M factor estimated by Eq. (15) has been assessed against the τ_M value derived from the numerical moment–curvature relationship obtained through a GMNIA analysis. Simply supported beams subjected to four-point loading conditions and bending around minor axis, as described in Section 2, were considered, and corresponded to the three stainless steel alloys shown in Table 1 and the cross-sections RHS1, RHS2 and RHS3 presented in Table 2. Bending moment–curvature relationships were determined at the midspan sections from the FE models, where the bending moment distribution is constant, and curvatures were calculated from Eq. (16), where u_{av} is the average value of the deflections at the loading sections, u_2 is the deflection at the midspan section and L_p is the distance between applied loads [47].

$$\kappa = \frac{8(u_2 - u_{av})}{4(u_2 - u_{av})^2 + {L_p}^2} \tag{16}$$

Fig. 4 shows the comparison between the stiffness reduction factor τ_M given in Eq. (15) for a RHS2 austenitic beam against the flexural stiffness reduction factor derived from GMNIA results. Suggested by Shen and

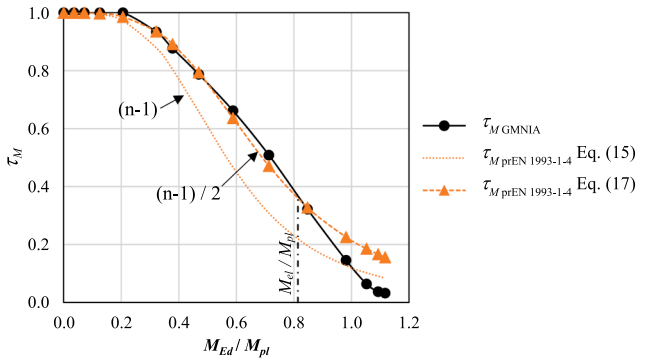

Fig. 4. Assessment of the proposed stiffness reduction factor τ_M for austenitic stainless steel beams under constant bending moment against the flexural stiffness reduction factor derived from GMNIA results (RHS2 cross-section).

Chacón [9], and as demonstrated in Fig. 4, substituting the term $(n-1)$ in Eq. (15) by $(n-1)/2$ provides a better fit of the analytical expression of τ_M. Consequently, the proposed stiffness reduction function τ_M is given in Eq. (17). As shown in Fig. 4, the fit obtained with Eq. (17) is excellent up to M_{el}, and becomes poorer beyond this value due to the strain hardening of the material.

$$\tau_M = \left[1 + (n-1)\frac{M_{el}}{M_{pl}}\left(\frac{M_{Ed}}{M_{pl}}\right)^{n-2}\right]^{-1} \tag{17}$$

4.2. Application of the proposed stiffness reduction factor τ_M

The accuracy of the proposed stiffness reduction function given in Eq. (17) was verified by means of FE analyses. A parametric analysis of simply supported beams following the four-point bending test configuration (4PB) was carried out. Beams bent about their minor axes, were 1500 mm long and vertical loads were applied at a distance of 510 mm away from the supports. Different materials corresponding to the three stainless steel families defined in Table 1 were analysed, considering three cross-sections (RHS1, RHS2 and RHS3 sections presented in Table 2) with varying local slenderness values for each material. Moment-curvature relationships were determined at the midspan sections as explained above. Fig. 5 shows the comparison of the proposed stiffness reduction factor τ_M given in Eq. (17) against the corresponding GMNIA results for austenitic, ferritic and duplex simply supported beams with RHS1 cross-section. The largest differences observed between the GMNIA and GNA-SR curves are in the cases of austenitic and duplex alloys. These discrepancies can be explained by the existing resistance reserve after M_{el} due to the strain hardening of the material, which the proposed stiffness reduction function τ_M does not take into account.

5. Stiffness reduction under combined axial load and bending

In this Section, a stiffness reduction function τ_{NM} that considers the detrimental effects of material nonlinearities, residual stresses and initial imperfections in stainless steel members under combined loading is presented. Results for a variety of beam-columns analysed according to the Stiffness Reduction Method (SRM) using the proposed τ_{NM} factor are also shown and assessed against the capacity of stainless steel benchmark members subjected to a combination of axial load and uniform bending. Finally, the consideration of different lineal moment distributions along the member length is addressed.

5.1. Proposal of stiffness reduction factor τ_{NM}

Kucukler et al. [29] proposed a stiffness reduction factor τ_{NM} to take into account the effect of yielding in I-section (IPE and HE) carbon steel

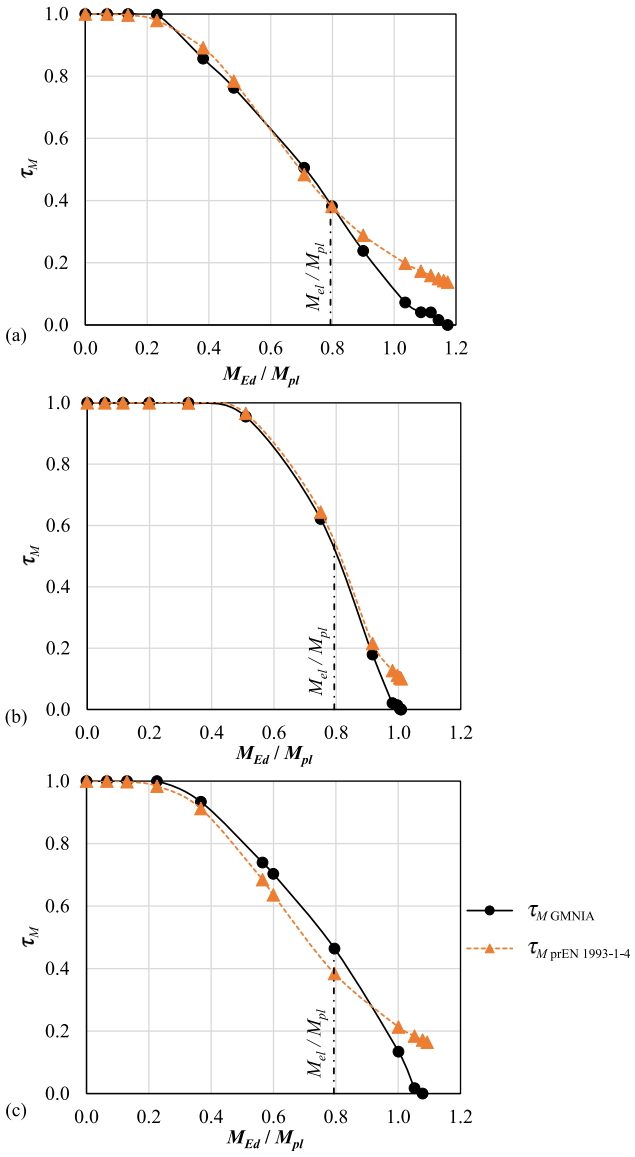

Fig. 5. Evaluation of the proposed reduction function τ_M for (a) austenitic, (b) ferritic and (c) duplex stainless steel simply supported beams under minor axis bending (RHS1 cross-section).

beams-columns subjected to a combination of axial load and uniform bending. The τ_{NM} expression proposed in [29] depends on two factors, which in turn depend on the cross-sectional aspect ratio H/B ($H/B \leq 1.2$ or > 1.2) and the axis of buckling and bending. The cross-sections studied in this paper are stainless steel rectangular hollow cross-sections (RHS) with $H/B > 1.2$. Since RHS cross-sections subjected to combined axial and uniaxial bending moment for both major and minor axes behave similarly to I-sections under axial load plus strong axis bending, the τ_{NM} factor proposed by Kucukler et al. [29] for carbon steel I-section beam-columns with $H/B > 1.2$ for combined axial load and major axis bending is adopted herein. Thus, the interaction stiffness reduction function τ_{NM} used in this study is given in Eq. (18), in which τ_N and τ_M correspond to the reduction factors determined from Eq. (7) and Eq. (17), respectively.

$$\tau_{NM} = \tau_N \tau_M \left\{1 - \left(\frac{N_{Ed}}{N_{pl}}\right)^{0.8}\left(\frac{M_{Ed}}{M_{pl}}\right)\right\} \tag{18}$$

5.2. Application of the proposed stiffness reduction factor τ_{NM}

A comprehensive parametric analysis on simply supported austenitic, ferritic and duplex stainless steel beam-columns subjected to axial load and uniform minor axis bending moment was conducted to assess the accuracy of the proposed τ_{NM} factor. Material properties considered in the FE models are shown in Table 1, and the details of the models have been discussed in Section 2. The member slenderness values considered were 0.5, 1.0 and 1.5, and the cross-sections analysed corresponded to the sections RHS1 and RHS2 defined in Table 2. Investigated bending moment-axial load ratios varied from pure compression to pure bending moment. Generally, constant bending moments were introduced by means of eccentric axial loads, with load eccentricity values equal to e_0 = 0.1*B*, 0.3*B*, 0.75*B*, 1.5*B*, *3.0B* and 9.0*B*, where *B* is the total cross-section width. Only in the cases with null axial loading (i.e., pure bending moment loading), members were subjected to equal bending moments applied at the endpoints.

The ultimate load and bending moment resistances of the beam-columns were obtained from a GNA-SR analysis using the τ_{NM} function proposed in Eq. (18) and following the procedure explained in Section 3.2. Since the local slendernesses of RHS1 and RHS2 are lower than 0.60, the ultimate applied loads N_{Ed} and corresponding bending moments M_{Ed} were determined from the GNA-SR analyses by applying the interaction equation given in Eq. (10) at the critical cross-sections. These values are compared with the ultimate strengths predicted from the GMNIA analyses in Fig. 6, which shows the nondimensional ultimate loads N_{Ed}/N_{pl} and bending moments M_{Ed}/M_{pl} predicted from the GNA-SR analyses using the proposed reduction factor τ_{NM} for simply supported beams-columns under uniform uniaxial bending for the cross-section RHS2, the three stainless steel families and the three member slenderness $\bar{\lambda}$ values considered. Ultimate capacities of restrained beam-columns predicted from the GMNIA analyses are also provided as benchmark. As mentioned in Section 3.1, the compression resistances in members are limited to the flexural buckling resistance values $N_{b,Rk}$, which are represented by dashed horizontal lines in Fig. 6, while the ultimate bending capacities are limited by the CSM bending resistance as Eq. (10) assumes M_{csm} as endpoint. Accurate and generally safe predictions are obtained for all materials and member slendernesses, since the GNA-SR predicted member strengths tend to lay below the GMNIA-predicted capacities. The most conservative estimations are obtained for stocky (i.e., short) specimens, since their structural behaviour is similar to that exhibited by the cross-section, without showing instability. In addition, when loading is governed by compressive loads, results seem to be more precise for austenitic alloys since, as discussed in Section 3.2, the austenitic buckling curve specified in the upcoming prEN 1993-1-4 [13] standard is in good agreement with the austenitic material used in the present study, while the buckling curves are worse fitted for the studied ferritic and duplex materials, as it was shown in Fig. 3.

It is worth emphasizing that the GNA-SR curves shown in Fig. 6 are very close to the GMNIA curves in those loading cases governed by bending moment, even if the proposed τ_M function gradually loses accuracy when $M_{Ed} > M_{el}$, as discussed in Section 4.1. Based on these results, it can be concluded that the τ_M factor defined by Eq. (17) accurately captures the stiffness loss of stainless steel beams subjected to constant bending up to a value of M_{csm}, and consequently a second stage of the formulation for τ_M is not necessary. This fact is especially valuable considering the simplicity of the proposed τ_M formula compared to those available in the literature [9,29].

In addition, the accuracy of the stiffness reduction function was assessed through the ratio ζ defined in Eq. (19), following the approach adopted in [30], which is the ratio between the radial distances measured from the origin to the normalised interaction GNA-SR (ζ_i) and GMNIA (ζ_{GMNIA}) curves.

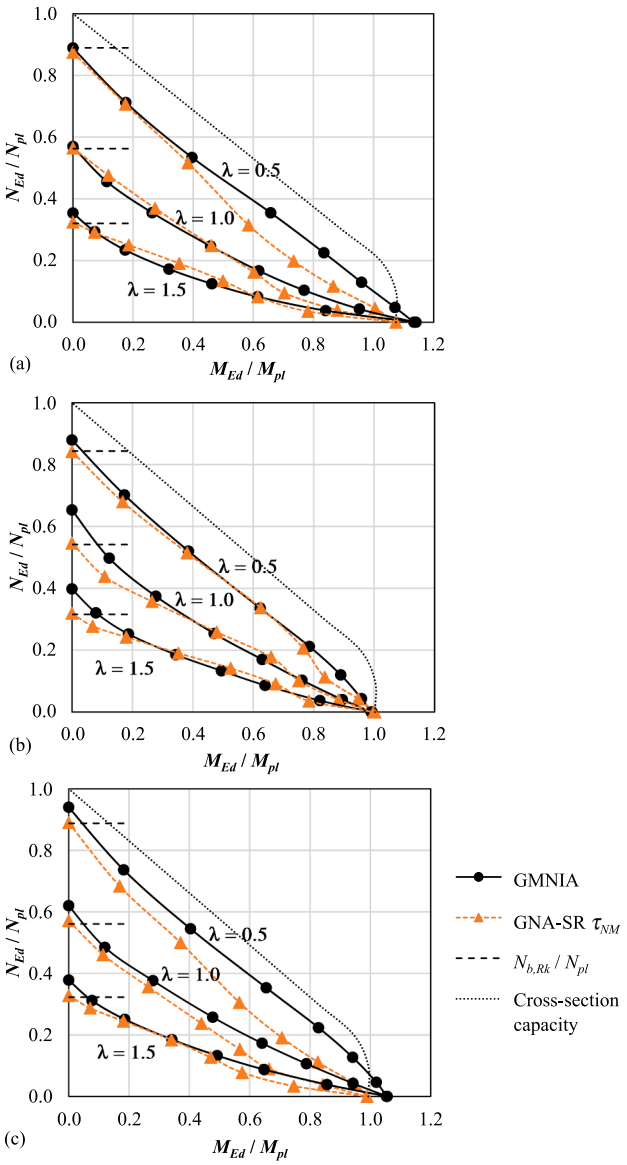

Fig. 6. Evaluation of GNA-SR results for (a) austenitic, (b) ferritic and (c) duplex stainless steel beam-columns under combined axial loading and uniform minor axis bending (RHS2 cross-section).

$$\zeta = \frac{\zeta_i}{\zeta_{GMNIA}} = \frac{\sqrt{\left(N_{Ed,i}/N_{pl}\right)^2 + \left(M_{Ed,i}/M_{pl}\right)^2}}{\sqrt{\left(N_{Ed,GMNIA}/N_{pl}\right)^2 + \left(M_{Ed,GMNIA}/M_{pl}\right)^2}} \tag{19}$$

Table 3 summarises the comparison of the ultimate capacities of GNA-SR with those of GMNIA, where ζ_{av} and ζ_{cov} are the average value and the coefficient of variation (COV) of the calculated ζ ratios for the different beam-columns investigated and the member slenderness considered, and ζ_{max} and ζ_{min} are the maximum and minimum ζ values. ζ values lower than 1.0 correspond to conservative predictions. As reported in Table 3, the GNA-SR method provides accurate ultimate strength predictions, with ζ_{av} values close to 1.0 and considerably small coefficients of variation (COV), especially in the cases of austenitic and ferritic beam-columns. However, the COV values tend to increase for increasing member slenderness $\bar{\lambda}$ values. It should be noted that the errors in the unconservative side (i.e., ζ values higher than 1.0) are usually not greater than 10% ($\zeta \leq 1.10$), and that only in the case of slender austenitic members subjected to similar proportions of bending moment and axial compression forces (see Fig. 6), the SRM exceeds

Table 3
Comparison of the ultimate capacities obtained through GNAR-SR and GMNIA analyses for simply supported beam-columns subjected to axial compression and uniform bending moment.

Stainless steel type	Cross-section type	$\bar{\lambda}$	ζ_{av}	ζ_{cov}	ζ_{max}	ζ_{min}
Austenitic	RHS1	0.5	0.99	0.022	1.02	0.95
		1.0	1.03	0.038	1.08	0.97
		1.5	1.05	0.073	1.16	0.90
	RHS2	0.5	0.94	0.043	0.99	0.88
		1.0	0.98	0.048	1.05	0.92
		1.5	1.00	0.068	1.11	0.92
Ferritic	RHS1	0.5	0.99	0.022	1.02	0.95
		1.0	0.97	0.080	1.07	0.83
		1.5	0.98	0.098	1.08	0.80
	RHS2	0.5	0.98	0.023	1.01	0.94
		1.0	0.96	0.070	1.05	0.84
		1.5	0.97	0.089	1.06	0.80
Duplex	RHS1	0.5	0.94	0.033	0.98	0.89
		1.0	0.95	0.039	1.00	0.89
		1.5	0.95	0.054	1.03	0.86
	RHS2	0.5	0.91	0.037	0.95	0.85
		1.0	0.91	0.037	0.95	0.84
		1.5	0.93	0.049	1.00	0.87

considerably the ultimate GMNIA strength (showing ζ_{max} values of 1.16 and 1.10). In contrast, the most conservative predictions are obtained for duplex members, with ζ_{max} values reported in Table 3 being always $\leq$ 1.0, and ζ_{min} values $\leq$ 0.85. For ferritic and duplex stainless steel members, the minimum ζ values are usually obtained under pure compression (i.e., for columns) because, as discussed in Section 3.2, the European buckling curves (and consequently τ_N) provide reasonable, but not perfect, ultimate member resistances for these materials.

5.3. Moment gradient effect

Consideration of the effects derived from bending moment gradients along the member length is assessed herein. To account for linear moment gradient variations, the proposed τ_{NM} function was modified applying an equivalent uniform moment factor C_m to the maximum bending moment along the member length M_{Ed}. Since the present work focuses on members with linear moment gradients, the expression for C_m developed by Austin [48] and shown in Eq. (20) is used, where μ is the ratio between the smaller and larger applied end moments. The effectiveness of this expression has been widely validated and it is the equivalent uniform moment factor adopted in EN 1993-1-1 [12].

$$C_m = 0.6 + 0.4\mu \text{ but } C_m \geq 0.4 \tag{20}$$

Therefore, Eq. (21) and Eq. (22) should be used in the calculation of τ_M and τ_{NM} instead of Eq. (17) and Eq. (18) to include the variation of bending moment in beam-columns.

$$\tau_M = \left[1 + (n-1)\frac{M_{el}}{M_{pl}}\left(\frac{C_m M_{Ed}}{M_{pl}}\right)^{n-2}\right]^{-1} \tag{21}$$

$$\tau_{NM} = \tau_N \tau_M \left\{1 - \left(\frac{N_{Ed}}{N_{pl}}\right)^{0.8}\left(\frac{C_m M_{Ed}}{M_{pl}}\right)\right\} \tag{22}$$

Fig. 7 shows the comparison between the GNA-SR and GMNIA results for two typical austenitic and duplex cases of simply supported beam-columns under axial load and varying minor axis bending along the length for cross-section RHS1. Linear bending moment distributions were obtained by applying an eccentricity only at one of the supports for the bending moment distribution corresponding to $\mu = 0$, and by applying load eccentricities with different signs at the two ends of the beam-columns for $\mu = -0.5$. GNA-SR predictions were limited by the cross-section interaction equation given in Eq. (10), as in the previous

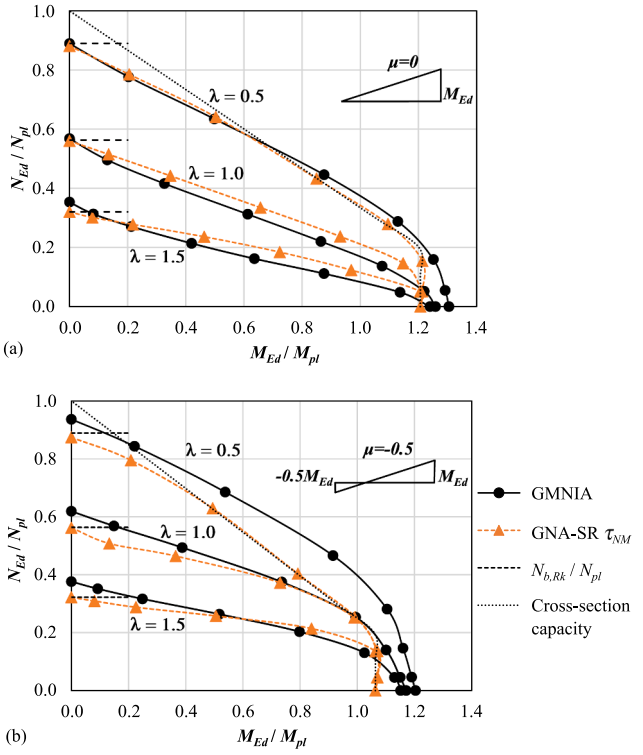

Fig. 7. Comparison of GNA-SR results for the proposed reduction factor for (a) austenitic and (b) duplex stainless steel beam-columns under combined axial loading and varying minor axis bending (RHS1 cross-section).

Sections. Similarly to the results reported in Table 3 for beam-columns under uniform bending moment, Table 4 summarises the ζ_{av}, ζ_{cov}, ζ_{max} and ζ_{min} values obtained from the comparison of the ultimate capacities predicted by the proposed GNA-SR approach with those of GMNIA for austenitic, ferritic and duplex beam-columns subjected to axial compression and bending moment gradients. It is worth noting that a number of the results shown in Fig. 7 and Table 4 for austenitic slender members, particularly under high bending and for the $\mu = -0.5$ distribution, are on the unsafe side, although deviations lie within the 10–18% range. This is because (1) the equivalent moment factor C_m neglects the influence of the member length and the level of axial load,

Table 4
Comparison of the ultimate capacities obtained through GNAR-SR and GMNIA analyses for simply supported beam-columns subjected to axial compression and gradient bending moment.

Specimen	Bending moment distribution μ	$\bar{\lambda}$	ζ_{av}	ζ_{cov}	ζ_{max}	ζ_{min}
Austenitic RHS1	0	0.5	0.97	0.030	1.01	0.92
		1.0	1.03	0.042	1.08	0.96
		1.5	1.03	0.074	1.14	0.91
	−0.5	0.5	0.94	0.042	1.00	0.89
		1.0	1.02	0.054	1.10	0.94
		1.5	1.02	0.097	1.18	0.91
Ferritic RHS1	0	0.5	0.97	0.021	0.99	0.94
		1.0	0.96	0.089	1.07	0.83
		1.5	0.96	0.103	1.09	0.80
	−0.5	0.5	0.95	0.018	0.98	0.92
		1.0	0.94	0.082	1.03	0.83
		1.5	0.94	0.104	1.06	0.80
Duplex RHS1	0	0.5	0.92	0.015	0.94	0.90
		1.0	0.95	0.030	1.00	0.91
		1.5	0.95	0.054	1.01	0.86
	−0.5	0.5	0.91	0.027	0.94	0.87
		1.0	0.94	0.039	1.00	0.89
		1.5	0.95	0.070	1.05	0.86

as previously highlighted in [49], which may lead to an overestimation of the beneficial effect of moment gradients on the beam-column stability, and (2) the proposed τ_M factor does not accurately capture the loss of stiffness due to material nonlinearity after M_{pl}, as discussed in Section 4, which is of particular relevance for austenitic beam-columns under the $\mu = -0.5$ distribution. Nevertheless, the analysis presented in Section 6 for austenitic portal frames indicates that good predictions of the ultimate frame strengths are obtained when the C_m factor is used in the analysis of structural systems, which is the relevant situation in design. The frames investigated covered the same ranges of member slenderness $\overline{\lambda}$ and μ factors considered in this Section. Besides, results in Table 4 indicate that, on average, GNA-SR results are in good agreement with those predicted by GMNIA for the bending moment distributions considered (i.e., ζ_{av} values are close to 1.0).

6. Stiffness reduction factors applied to portal frame design

In this Section, the proposed stiffness reduction factor τ_{NM} is applied to the in-plane design of stainless steel portal frames. The assessment of the Stiffness Reduction Method was carried out through the comparison of the ultimate loads obtained for the τ_{NM} factor proposed in this paper with those determined using the Direct Analysis Method prescribed in the AISC 370 [25] Specification and the ultimate strengths predicted from GMNIA analyses.

6.1. Application of the proposed method for in-plane global design

The accuracy of the proposed Stiffness Reduction Method (SRM) to predict the global behaviour of stainless steel structures was assessed through a parametric study comprising austenitic RHS portal frames. A total of 20 single-span in-plane frames were studied: the height (L_c) of all columns was 2 m, while the span lengths (L_b) varied from 2 m to 4 m. All members featured the austenitic stainless steel material properties reported in Table 1 and the RHS1 cross-section given in Table 2, oriented in such a way that all members bent about their major axes. The loading scheme, shown in Fig. 8, ensured that the most loaded cross-sections were located at the columns in all frames. Both fixed- and pin-ended support conditions were analysed and vertical (V_{Ed}) and horizontal (H_{Ed}) loads were applied simultaneously in different proportions at the top of the columns. Table 5 summarises the horizontal load H_{Ed} values studied as a function of the applied vertical load V_{Ed}. Note that $H_{Ed} = 0$ and $V_{Ed} = 0$ imply that the portal frame was loaded only vertically or horizontally, respectively. Member slenderness values $\overline{\lambda}$ ranged from 1.01 to 2.29, while bending moment distribution factors were $\mu = -1$ for beams, and $\mu = [-0.59, -0.74]$ and $\mu = 0$ for fixed- and pin-ended columns, respectively, which are in line with the beam-column cases analysed in Section 5.3.

The frames described above were analysed using the SRM proposed herein, i.e., by performing GNA-SR analyses on the numerical models described in Section 2.1.3, and the predicted ultimate capacities and internal forces were compared to those estimated from GMNIA. The

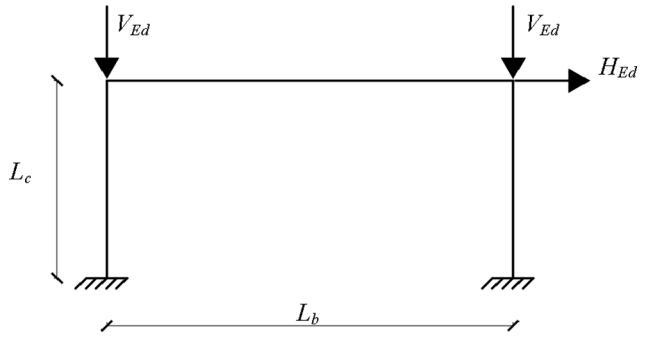

Fig. 8. Loading scheme for austenitic stainless steel portal frames.

Table 5
Frame cases analysed.

Frame case No.	Boundary conditions	$L_c \times L_b$	Horizontal loading H_{Ed}
1–12	Fixed-ended	2 × 4 m 2 × 2 m	$H_{Ed} = 0$, $0.03V_{Ed}$, $0.01V_{Ed}$, $0.25V_{Ed}$, $1.0V_{Ed}$, $V_{Ed} = 0$
13–20	Pin-ended	2 × 4 m 2 × 2 m	$H_{Ed} = 0$, $0.01V_{Ed}$, $1.0V_{Ed}$, $V_{Ed} = 0$

application of the SRM to obtain the ultimate load of a structure is an iterative process, as stiffness reduction factors should be calculated for the load levels at which cross-section capacities are checked, and re-run until the capacity of the cross-sections is fully utilised [26,30]. In the GNA-SR analysis, the flexural stiffness of each member was reduced by the corresponding τ_{NM} factor determined from Eq. (22), where the factors τ_N and τ_M were obtained from Eq. (7) and Eq. (21). The GNA-SR analysis was conducted until the most loaded section of the frame reached its resistance capacity, evaluated from the cross-section interaction equation Eq. (10), since RHS1 exhibits a local slenderness lower than 0.60. For the studied pin-ended frames, the critical sections were located at the beam-to-column joints, while for the fixed-ended frames the critical sections were those at the supports of the columns. Note that since the GMNIA analyses were carried out on beam-type FE models (as explained in Section 2.1.2), the frame strengths and target internal forces were also obtained by checking the resistances of the critical cross-sections through the same Eq. (10) used for SRM analyses.

For assessment purposes, the 20 single-span in-plane frames were also analysed following the Direct Analysis Method (DM) prescribed in AISC 370 [25] for the design of stainless steel structures, in which the flexural stiffness of the members is adjusted by two different factors, τ_g and τ_b. The first factor τ_g corresponds to a general stiffness reduction, which is applied to all members and accounts for the reduction in member stiffness due to the development and spread of plasticity. A constant value of $\tau_g = 0.7$ is adopted for all stainless steel members, as proposed in [26]. The second factor τ_b is an additional factor that is applied to the stiffness of those members that contribute to the stability of the structure. τ_b is given by Eq. (23) when considering the Load and Resistance Factor Design (LRFD) approach and was derived from the Ramberg-Osgood expression, so it considers the further loss in stiffness due to material nonlinearities, and it also takes into account the detrimental effect of residual stresses by means of the effective strain hardening exponent n_{eff}. The value of n_{eff} depends on the strain hardening coefficient n, the cross-section type and the buckling axis, and was proposed in [26] and is tabulated in AISC 370 [25]. For the case of rectangular hollow sections studied herein, n_{eff} assumes a value equal to the strain hardening coefficient n, as the effects of residual stresses is negligible [26].

$$\tau_b = \frac{1.0}{1.0 + 0.002 n_{eff} \frac{E}{f_y} \left(\frac{N_{Ed}}{N_{pl}} \right)^{n_{eff}-1}} \tag{23}$$

There are three potential design options in AISC 370 [25] when the DM is adopted: (1) not including member imperfections explicitly in the structural analysis and verifying the structure by checking member capacities, (2) including member imperfections in the analysis and verifying the capacity of the structure through cross-section strength equations that use the plastic section capacities N_{pl} and M_{pl}, and (3) including member imperfections in the analysis and verifying the capacity of the structure through cross-section checks that are anchored to the more accurate CSM end-points. Both member and cross-section checks should follow the corresponding design provisions prescribed in AISC 370 [25]. In the comparisons carried out in this paper, the latter approach is adopted because it is the option that is most similar to the GNA-SR proposal presented. Notional loads were used to include initial global imperfections with a value equal to $0.002N_{Ed}$, which is based on a

nominal initial storey out-of-plumbness ratio of 1/500 according to AISC 370 [25], while member imperfections were included in the beam-type FE models by directly modifying the position of the nodes following a half-sine wave shape with an amplitude of $L_c/1000$ in the most detrimental direction, as for the GMNIA models described in Section 2.1.2. Note that although the nominal out-of-plumbness ratio adopted for the DM is slightly lower than the corresponding value used in the GNA-SR analyses, the member imperfection amplitudes are equivalent, since the imperfection amplitude used in the calibration of the European buckling curves was $L_c/1000$. Since member instability is directly accounted for in the analysis, the capacity of the structure is verified by means of cross-section checks. Eq. (24) and Eq. (25) show the CSM cross-section interaction equations provided in AISC 370 [25], where N_{Ed} and M_{Ed} are the second-order internal axial force and bending moment obtained from the DM at the critical sections, and $P_{n,csm}$ and $M_{n,csm}$ are the CSM cross-section resistances in compression and bending, respectively. Note that the AISC 370 $P_{n,csm}$ and $M_{n,csm}$ capacities are based on the same CSM base curve given in Eq. (9), but adopt a lower value of 5 for the Ω parameter [25,26]. Formulae to calculate $P_{n,csm}$ and $M_{n,csm}$ are provided in [25,26]. In the present study partial safety and resistance factors proposed in prEN 1993-1-4 [13] and AISC 370 [25] assume values equal to unity.

$$\frac{N_{Ed}}{P_{n,csm}}+\frac{8}{9}\frac{M_{Ed}}{M_{n,csm}}\leq 1.0 \quad \text{for} \quad N_{Ed}\geq 0.2P_{n,csm} \tag{24}$$

$$\frac{N_{Ed}}{2P_{n,csm}}+\frac{M_{Ed}}{M_{n,csm}}\leq 1.0 \quad \text{for} \quad N_{Ed}< 0.2P_{n,csm} \tag{25}$$

6.2. Assessment of the results

The ultimate load predictions obtained with the proposed SRM for stainless steel frames subjected to combined vertical and horizontal loads are summarised in Fig. 9, where the results plotted in Fig. 9(a) correspond to large span frames and in Fig. 9(b) to short span frames. Both figures show the SRM predictions for fixed- and pin-ended boundary conditions, as well as the AISC 370-DM [25] predictions and the GMNIA results for reference. In addition, Table 6 reports the values of the stiffness reduction factors for each member of the studied frames, according to the proposed SRM ($\tau_{NM,i}$) and the AISC 370-DM ($\tau_g\tau_{b,i}$) approaches, where the subscripts *l*, *r* and *b* refer to the left column, the right column and the beam, respectively. Note that for all the cases analysed in this paper, the AISC 370-DM stiffness reduction factor for the beams is equal to $\tau_g\tau_{b,b}=\tau_g=0.70$. Similar stiffness reduction factors and ultimate capacities were estimated for large span frames and short span frames, and the differences were associated with the type of boundary condition and load combinations. Following the approach given in [30], Table 6 also provides the parameter ζ, which refers to the accuracy of the considered method for the prediction of the ultimate frame strengths. The factor ζ is determined using Eq. (19), where M_{Ed} refers to the bending moment in the column and the subscript *i* refers to the assessed method (i.e., the proposed SRM or the AISC 370-DM approach). Recall that ζ values lower than 1.0 correspond to conservative predictions. According to the results shown in Fig. 9 and Table 6, the proposed SRM accurately predicts the ultimate capacities of the frames. Only in the case of high vertical loads, in which the structural behaviour of the frames is determined by the buckling of their columns in compression, the SRM slightly underestimates the GMNIA strength predictions. While in the GMNIA analyses the vertical reaction observed in the supports were higher than the flexural buckling resistances $N_{b,Rk}$, in the SRM the column capacities were limited to $N_{b,Rk}$, as discussed in Section 3.1. In any case, the predictions obtained by the proposed SRM are adequate and provide a reasonable safety margin. Accurate and safe results are also obtained when using the AISC 370-DM [25] approach studied herein, although the ultimate capacity of fixed-ended frames is slightly underestimated, as shown in Fig. 9. The discrepancies between the two approaches are partly due to the use of different strength interaction equations to limit the GNA-SR analyses, but mainly to the fact that the CSM base curve adopts a different limiting value for Ω in the two approaches (i.e., Ω = 15 in prEN 1993-1-4 [13] but Ω = 5 in AISC 370-DM [25]). Regarding the interaction equations, even if the AISC 370-DM equations are anchored to the CSM cross-section resistances, they are more restrictive than the cross-section interaction check used in the proposed SRM (Eq. (10)) because they adopt a linear interaction function. On the other hand, as the RHS1 cross-section used in this study for the assessment of the design approaches is very stocky, the CSM strain in Eq. (9) is limited by the parameter Ω in the two approaches, which adopts different values (i.e., Ω = 5 for the DM as opposed to Ω = 15 for the SRM), and thus the CSM bending moment resistances M_{csm} are significantly different. This can be clearly observed for the cases of fixed-ended portal frames with $V_{Ed}=0$, where the frames are almost entirely bending dominated and the differences in interaction equation have almost no consequence, and the results are governed in both cases by the CSM bending moment resistance M_{csm}. Since the SRM approach proposed in this paper uses a less restrictive ductility limit of Ω = 15, the value of M_{csm}, and thus the predicted capacity of the frames, is higher. Nevertheless, for less stocky cross-sections, where the CSM strain would not be determined by the Ω limit, more similar values of M_{csm} would be obtained for the two approaches and the results obtained from the proposed SRM and the AISC 370-DM would be less different.

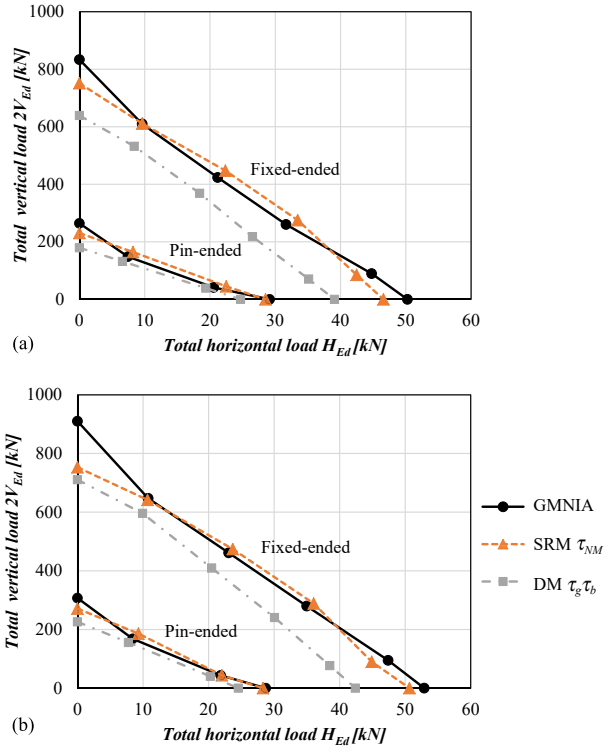

Fig. 9. Assessment of the results for the proposed stiffness reduction factors against GMNIA results and the DM [25] for austenitic stainless steel in-plane portal frames with (a) L_b = 4 m and (b) L_b = 2 m under vertical and horizontal loading (RHS1 cross-section).

The accuracy of the SRM and DM approaches for the prediction of internal forces was also assessed according to the indications given in [30], i.e., through the comparison of the nondimensional internal forces $N_{Ed,i}/N_{pl}$ - $M_{Ed,i}/M_{pl}$ obtained from the considered method (i.e., the proposed SRM or the AISC 370-DM approach) and those obtained from the GMNIA analysis at the critical sections of the columns using Eq. (19). Results of the accuracy for the different design methods are summarised in Table 7, where ζ_{av} and ζ_{cov} are the average and coefficient of variation (COV) of ζ, and ζ_{max} and ζ_{min} are the maximum and minimum ζ values for the internal forces registered in the columns. As shown in Table 7, the

Table 6
Assessment of the accuracy of the proposed stiffness reduction method SRM and the DM for the prediction of ultimate strengths in austenitic stainless steel portal frames.

Frame case	Horizontal loading H_{Ed}	SRM				AISC 370-DM			
		$\tau_{NM,l}$	$\tau_{NM,r}$	$\tau_{NM,b}$	ζ	$\tau_g\tau_{b,l}$	$\tau_g\tau_{b,r}$	$\tau_g\tau_{b,b}$	ζ
2 × 4 m	$H_{Ed} = 0$	0.61	0.61	1.00	0.91	0.59	0.59	0.70	0.77
Fixed-ended	$0.03V_{Ed}$	0.66	0.66	0.96	1.00	0.68	0.68	0.70	0.87
	$0.01V_{Ed}$	0.70	0.69	0.92	1.05	0.70	0.70	0.70	0.87
	$0.25V_{Ed}$	0.72	0.70	0.91	1.05	0.70	0.70	0.70	0.84
	$1.0V_{Ed}$	0.70	0.68	0.87	0.94	0.70	0.70	0.70	0.78
	$V_{Ed} = 0$	0.71	0.71	0.84	0.92	0.70	0.70	0.70	0.78
2 × 2 m	$H_{Ed} = 0$	0.56	0.55	1.00	0.83	0.54	0.54	0.70	0.78
Fixed-ended	$0.03V_{Ed}$	0.64	0.63	0.96	0.99	0.67	0.67	0.70	0.92
	$0.01V_{Ed}$	0.69	0.67	0.93	1.02	0.70	0.69	0.70	0.89
	$0.25V_{Ed}$	0.71	0.68	0.89	1.03	0.70	0.70	0.70	0.86
	$1.0V_{Ed}$	0.73	0.67	0.83	0.94	0.70	0.70	0.70	0.81
	$V_{Ed} = 0$	0.71	0.70	0.79	0.95	0.70	0.70	0.70	0.80
2 × 4 m	$H_{Ed} = 0$	0.81	0.81	1.00	0.88	0.70	0.70	0.70	0.68
Pin-ended	$0.01V_{Ed}$	0.81	0.80	0.96	1.10	0.70	0.70	0.70	0.89
	$1.0V_{Ed}$	0.66	0.62	0.86	1.08	0.70	0.70	0.70	0.94
	$V_{Ed} = 0$	0.39	0.39	0.70	0.97	0.70	0.70	0.70	0.85
2 × 2 m	$H_{Ed} = 0$	0.79	0.79	1.00	0.89	0.70	0.70	0.70	0.74
Pin-ended	$0.01V_{Ed}$	0.79	0.77	0.96	1.09	0.70	0.70	0.70	0.93
	$1.0V_{Ed}$	0.65	0.55	0.84	1.00	0.70	0.70	0.70	0.93
	$V_{Ed} = 0$	0.38	0.38	0.71	0.98	0.70	0.70	0.70	0.85

Table 7
Comparison of the accuracy of the SRM and DM approaches for the prediction of internal forces in the critical column of the frame cases analysed.

Method	ζ_{av}	ζ_{cov}	ζ_{max}	ζ_{min}
SRM	1.00	0.010	1.02	0.98
AISC 370-DM	0.85	0.026	0.88	0.80

internal forces predicted by the proposed SRM approach are in good agreement with those considered as target values ($\zeta_{av} = 1.00$ and $\zeta_{cov} = 0.010$), while the results obtained for the DM approach are slightly more conservative and more scattered ($\zeta_{av} = 0.85$ and $\zeta_{cov} = 0.026$). Based on the reported results, it can be concluded that the proposed SRM and the AISC 370-DM [25] approach analysed herein provide safe predictions of the ultimate in-plane response of stainless steel frames with stocky RHS sections under combined vertical and horizontal loads, but slightly better results are obtained for the proposed SRM approach, especially for fixed-ended frames. In addition, the proposal has the advantage of not requiring the explicit introduction of member imperfections in the numerical models. Finally, it is important to note that the ultimate capacity of the structure obtained by either method will be generally lower than the ultimate load predicted from a GMNIA analysis since both methods are limited to the development of the first plastic hinge without considering any redistribution of internal forces.

7. Summary of the proposed Stiffness Reduction Method

The procedure to apply the proposed Stiffness Reduction Method for the in-plane stability design of stainless steel structures with stocky RHS sections is summarised as follows:

(i) Perform a Linear Elastic Analysis (LA) to estimate the maximum internal forces (axial force N_{Ed} and bending moment M_{Ed}) in each member under the design loads.
(ii) Calculate the Stiffness Reduction factors for each member from the proposed formulae:

$$\tau_N = \frac{4\psi^2}{\alpha^{2\frac{N_{Ed}}{N_{pl}}}\left[1+\sqrt{1-4\psi\frac{\left(N_{Ed}/N_{pl}-1\right)}{\alpha^2 N_{Ed}/N_{pl}}}\right]^2} \quad \text{but } \tau_N \le 1 \tag{7}$$

where

$$\psi = 1 + \bar{\lambda}_0\alpha\frac{N_{Ed}}{N_{pl}} - \frac{N_{Ed}}{N_{pl}} \tag{8}$$

$$\tau_M = \left[1+(n-1)\frac{M_{el}}{M_{pl}}\left(\frac{C_m M_{Ed}}{M_{pl}}\right)^{n-2}\right]^{-1} \tag{21}$$

$$\tau_{NM} = \tau_N\tau_M\left\{1-\left(\frac{N_{Ed}}{N_{pl}}\right)^{0.8}\left(\frac{C_m M_{Ed}}{M_{pl}}\right)\right\} \tag{22}$$

where

$$C_m = 0.6 + 0.4\mu \quad \text{but} \quad C_m \ge 0.4 \tag{20}$$

With $\bar{\lambda}_0$ and α being the slenderness plateau and imperfection factor given in next version of prEN 1993-1-4 [13], respectively; and μ being the ratio between the smaller and larger applied end moments.

(iii) Perform a Geometrically Nonlinear Analysis with Stiffness Reduction (GNA-SR) considering initial global imperfections (out-of-plumbness) only. Note that stiffness reduction factors should affect the flexural stiffnesses, but not the axial stiffnesses, of the members.
(iv) Check the cross-section capacity using the internal forces determined from the GNA-SR analysis under the design loads through the following strength interaction expression for stocky sections:

$$M_{Ed} \le M_N = M_{csm}\frac{1-\left(N_{Ed}/N_{pl}\right)}{1-0.5a} \le M_{csm} \quad \text{for} \quad \lambda_p \le 0.60 \tag{10}$$

8. Conclusions

A Stiffness Reduction Method for the in-plane stability design of stocky RHS stainless steel structures based on the provisions included in the upcoming version of the prEN 1993-1-4 [13] standard has been

presented. The proposed approach allows predicting the ultimate capacity and internal forces in stainless steel structures by performing a second-order elastic analysis in which the stiffness of members is reduced by a set of factors defined in this paper to account for the effect of the spread of plasticity, residual stresses and member imperfections. The method only requires that initial out-of-plumbness imperfections be included, and the verification is limited to checking cross-section capacities. The proposed stiffness reduction factors consider the loss of stiffness in members and planar structures due to axial load, uniaxial bending and the combination of axial loading and uniaxial bending effects. The stiffness reduction factors under axial loads are derived from the European buckling curves and the reduction factors under bending are based on an analytical moment–curvature model developed in this paper. A third reduction factor under combined axial load and bending moment based on the previous ones is also proposed, which accounts for different bending moment distributions along the member.

The accuracy of these factors has been evaluated by comparing the strengths estimated numerically for RHS stainless steel columns, beams and beam-columns, which showed a good agreement with GMNIA results. Furthermore, the proposed stiffness reduction factors have been applied to the in-plane design of austenitic stainless steel portal frames with different boundary conditions and load combinations. It has been found that, for most of the studied cases, the ultimate strengths and internal forces predicted by the proposed Stiffness Reduction Method coincide with the benchmark strengths of the structures determined from GMNIA analyses. In addition, the assessment of the results has shown that comparable strength capacities are obtained using the Direct Analysis Method approach that will be included in the upcoming AISC 370 [25] Specification for stainless steel structures, which is based on second-order analysis with member imperfections and adopts CSM-based cross-section checks.

To fully consider the proposed Stiffness Reduction Method as an alternative approach to improve and simplify the stability design of stainless steel frames according to European provisions, the present study should be extended to other cross-section types, including slender cross-sections prone to local buckling, other failure modes and load combinations, such as lateral-torsional buckling and axial load plus biaxial bending, respectively, as well as to more complex structures.

CRediT authorship contribution statement

Isabel González-de-León: Conceptualization, Methodology, Software, Formal analysis, Data curation, Writing – original draft. **Itsaso Arrayago:** Conceptualization, Methodology, Formal analysis, Writing – original draft. **Esther Real:** Conceptualization, Supervision, Writing – review & editing. **Enrique Mirambell:** Supervision, Writing – review & editing.

Declaration of Competing Interest

The authors declare that they have no known competing financial interests or personal relationships that could have appeared to influence the work reported in this paper.

Acknowledgements

The research presented in this paper was developed in the frame of the Project BIA2016-75678-R, AEI/FEDER, UE “Comportamiento estructural de pórticos de acero inoxidable. Seguridad frente a acciones accidentales de sismo y fuego”, funded from the MINECO (Spain). The financial support received from the Spanish Ministry for Science, Innovation and Universities through the FPI-MINECO PhD fellowship Ref. BES-2017-082958 (I. González-de-León) and from the European Commission through the Marie Sklodowska-Curie grant agreement No. 842395 (I. Arrayago) is also gratefully acknowledged.

References

[1] Afshan S, Gardner L. The continuous strength method for structural stainless steel design. Thin-Walled Struct 2013;68:42–9.
[2] Bock M, Gardner L, Real E. Material and local buckling response of ferritic stainless steel sections. Thin-walled Struct 2015;89:131–41.
[3] Zhao O, Afshan S, Gardner L. Structural response and continuous strength method design of slender stainless steel cross-sections. Eng Struct 2017;140:14–25.
[4] Arrayago I, Rasmussen KJR, Real E. Full slenderness range DSM approach for stainless steel hollow cross-section columns and beam-columns. J Constr Steel Res 2017;138:246–63.
[5] American Society of Civil Engineers (ASCE). SEI/ASCE 8-02. Specification for the design of cold-formed stainless steel structural members. Reston, USA; 2002.
[6] European Committee for Standardization (CEN). EN 1993-1-4:2006+A1. Eurocode 3: Design of steel structures – Part 1-4: General rules. Supplementary rules for stainless steels, including amendment A1. Brussels, Belgium; 2015.
[7] Walport F, Gardner L, Real E, Arrayago I, Nethercort DA. Effects of material nonlinearity on the global analysis and stability of stainless steel frames. J Constr Steel Res 2019;152:173–89.
[8] Arrayago I, González-de-León I, Real E, Mirambell E. Tests on stainless steel frames. Part II: Results and analysis. Thin-Walled Struct 2020;157:107006.
[9] Shen YF, Chacón R. Geometrically Nonlinear Analysis with stiffness reduction for the stability design of stainless steel structures: application to members and planar frames. Thin-Walled Structures 2020;148:106581.
[10] González-de-León I, Arrayago I, Real E. Interaction of geometric and material nonlinearities in stainless steel frames. In: 9th European conference on steel and composite structures Eurosteel 2021. Sheffield, UK; 2021. p. 2149–2157.
[11] European Committee for Standardization (CEN). prEN 1993-1-14. Eurocode 3: Design of steel structures – Part 1-14: Design assisted by finite element analysis. Brussels, Belgium; 2021.
[12] European Committee for Standardization (CEN). EN 1993-1-1. Eurocode 3 – Design of steel structures – Part 1-1: General rules and rules for buildings. Brussels, Belgium; 2005.
[13] European Committee for Standardization (CEN). prEN 1993-1-4. Eurocode 3: Design of steel structures – Part 1-4: General rules. Supplementary rules for stainless steels. Brussels, Belgium; 2021.
[14] Liew JYR, White DW, Chen WF. Second-order refined plastic-hinge analysis for frame design. Part I. J Struct Eng (ASCE) 1993;119(11):3196–216.
[15] Liew JYR, White DW, Chen WF. Second-order refined plastic-hinge analysis for frame design. Part II. J Struct Eng (ASCE) 1993;119(11):3217–36.
[16] Ziemian RD, McGuire W. Modified tangent modulus approach, a contribution to plastic hinge analysis. J Struct Eng (ASCE) 2002;128(10):1301–7.
[17] Zubydan AH. A simplified model for inelastic second order analysis of planar frames. Eng Struct 2010;32(10):3258–68.
[18] Zubydan AH. Inelastic second order analysis of steel frame elements flexed about minor axis. Eng Struct 2011;33(4):1240–50.
[19] Kim SE, Chen WF. Practical advanced analysis for braced steel frame design. J Struct Eng (ASCE) 1996;122(11):1266–74.
[20] Kim SE, Chen WF. Practical advanced analysis for unbraced steel frame design. J Struct Eng (ASCE) 1996;122(11):1259–65.
[21] Surovek-Maleck AE, White DW. Alternative approaches for elastic analysis and design of steel frames. I: overview. J Struct Eng (ASCE) 2004;130(8):1186–96.
[22] Surovek-Maleck AE, White DW. Alternative approaches for elastic analysis and design of steel frames. II: verification studies. J Struct Eng (ASCE) 2004;130(8):1197–205.
[23] American Institute of Steel Construction (ANSI/AISC). AISC 360. Specification for structural steel buildings. Illinois, USA; 2016.
[24] Ziemian RD. Guide to stability design criteria for metal structures. John Wiley & Sons; 2010.
[25] American Institute of Steel Construction (ANSI/AISC). AISC 370. Specification for Structural Stainless Steel Buildings. Illinois, USA; 2021. *Draft for public review*.
[26] Walport F, Kucukler M, Gardner L. Stability design of stainless steel structures. J Struct Eng (ASCE) 2021;148(1):04021225.
[27] Landesmann A, Batista EM. Advanced analysis of steel framed buildings using the Brazilian standard and Eurocode-3. J Constr Steel Res 2005;61(8):1051–74.
[28] Barszcz AM, Gizejowski MA. An equivalent stiffness approach for modelling the behaviour of compression members according to Eurocode 3. J Constr Steel Res 2007;63(1):55–70.
[29] Kucukler M, Gardner L, Macorini L. A stiffness reduction method for the in-plane design of structural steel elements. Eng Struct 2014;73:72–84.
[30] Kucukler M, Gardner L, Macorini L. Development and assessment of a practical stiffness reduction method for the in-plane design of steel frames. J Constr Steel Res 2016;126:187–200.
[31] Abaqus. ABAQUS/Standard user’s manual volumes I-III and ABAQUS CAE manual. Dassault Systemes Simulia Corporation; 2014.
[32] Li HT, Young B. Web crippling of cold-formed ferritic stainless steel square and rectangular hollow sections. Eng Struct 2018;176:968–80.
[33] Theofanous M, Gardner L. Testing and numerical modelling of lean duplex stainless steel hollow section columns. Eng Struct 2009;31(12):3047–58.
[34] Arrayago I, Picci F, Mirambell E, Real E. Interaction of bending and axial load for ferritic stainless steel RHS columns. Thin-Walled Struct 2015;91:96–107.
[35] Gardner L, Nethercot DA. Numerical modeling of stainless steel structural components – a consistent approach. J Struct Eng (ASCE) 2004;130(10):1586–601.
[36] Arrayago I, Real E, Mirambell E. Design of stainless steel continuous beams with tubular cross-sections. Eng Struct 2017;151:422–31.

[37] Arrayago I, González-de-León I, Real E, Mirambell E. Tests on stainless steel frames. Part I: Preliminary tests and experimental set-up. Thin-Walled Struct 2020; 157:107005.
[38] Walport F, Gardner L, Nethercot DA. Design of structural stainless steel members by second order inelastic analysis with CSM strain limits. Thin-Walled Struct 2021; 159:107267.
[39] Meza FJ, Baddoo NR, Gardner L. Development of flexural buckling rules for the new AISC stainless steel design specification. In: 9th European conference on steel and composite structures Eurosteel 2021. Sheffield, UK; 2021. p. 1537–1542.
[40] Arrayago I, Real E, Gardner L. Description of stress-strain curves for stainless steel alloys. Mater Des 2015;87:540–52.
[41] Arrayago I, Real E, Mirambell E, Gardner L. The Continuous Strength Method for the design of stainless steel hollow section columns. Thin-Walled Struct 2020;154: 106825.
[42] Steel Construction Institute (SCI). Design manual for structural stainless steel, fourth ed.; 2017.
[43] Maquoi R, Rondal J. Mise en équation des nouvelles courbes Européennes deflambement. Construct Métallique 1978;1:17–30.
[44] Li Z, Schafer BW. Buckling analysis of cold-formed steel members with general boundary conditions using CUFSM: conventional and constrained finite strip methods. In: 20th International speciality conference on cold-formed steel structures. Saint Louis, Missouri, USA; 2010.
[45] Real E, Mirambell E. Flexural behaviour of stainless steel beams. Eng Struct 2005; 27:1465–75.
[46] Arrayago I, Rasmussen KJR. Buckling curves for cold-formed stainless steel columns and beams. J Struct Eng (ASCE) 2021;147(10):04021149.
[47] Rasmussen KJR, Hancock GJ. Design of cold formed stainless steel structural members. II: beams. J Struct Eng (ASCE) 1993;119(8):2368–86.
[48] Austin WJ. Strength and design of metal beam-columns. J Struct Div 1961;87(4): 1–32.
[49] Zhao O, Gardner L, Young B. Experimental study of ferritic stainless steel tubular beam-column members subjected to unequal end moments. J Struct Eng (ASCE) 2016;142(11):04016091.